

# Most stringent bound on electron neutrino mass obtained with a scalable low temperature microcalorimeter array

B.K. Alpert,<sup>1</sup> M. Balata,<sup>2</sup> D.T. Becker,<sup>3</sup> D.A. Bennett,<sup>1</sup> M. Borghesi,<sup>4, 5, \*</sup> P. Campana,<sup>4, 5</sup>  
R. Carobene,<sup>4, 5</sup> M. De Gerone,<sup>6</sup> W.B. Doriese,<sup>1</sup> M. Faverzani,<sup>4, 5</sup> L. Ferrari Barusso,<sup>7, 6</sup> E. Ferri,<sup>5</sup>  
J.W. Fowler,<sup>1</sup> G. Gallucci,<sup>6</sup> S. Gamba,<sup>4, 5</sup> J.D. Gard,<sup>3</sup> F. Gatti,<sup>7, 6</sup> A. Giachero,<sup>4, 5</sup> M. Gobbo,<sup>4, 5</sup>  
U. Köster,<sup>8</sup> D. Labranca,<sup>4, 5</sup> M. Lusignoli,<sup>9, 10</sup> P. Manfrinetti,<sup>11</sup> J.A.B. Mates,<sup>1</sup> E. Maugeri,<sup>12</sup>  
R. Moretti,<sup>4, 5</sup> S. Nisi,<sup>2</sup> A. Nucciotti,<sup>4, 5, †</sup> G.C. O’Neil,<sup>1</sup> L. Origo,<sup>4, 5</sup> G. Pessina,<sup>5</sup> S. Ragazzi,<sup>4, 5</sup>  
C.D. Reintsema,<sup>1</sup> D.R. Schmidt,<sup>1, ‡</sup> D. Schumann,<sup>12</sup> D.S. Swetz,<sup>1</sup> Z. Talip,<sup>12</sup> J.N. Ullom,<sup>1, §</sup> and L.R. Vale<sup>1</sup>

<sup>1</sup>*National Institute of Standards and Technology (NIST), Boulder, Colorado, USA*

<sup>2</sup>*Laboratori Nazionali del Gran Sasso (LNGS), INFN, Assergi (AQ), Italy*

<sup>3</sup>*University of Colorado, Boulder, Colorado, USA*

<sup>4</sup>*Dipartimento di Fisica, Università di Milano-Bicocca, Milano, Italy*

<sup>5</sup>*Istituto Nazionale di Fisica Nucleare (INFN), Sezione di Milano-Bicocca, Milano, Italy*

<sup>6</sup>*Istituto Nazionale di Fisica Nucleare (INFN), Sezione di Genova, Genova, Italy*

<sup>7</sup>*Dipartimento di Fisica, Università di Genova, Genova, Italy*

<sup>8</sup>*Institut Laue-Langevin (ILL), Grenoble, France*

<sup>9</sup>*Istituto Nazionale di Fisica Nucleare (INFN), Sezione di Roma 1, Roma, Italy*

<sup>10</sup>*Dipartimento di Fisica, Sapienza, Università di Roma, Roma, Italy*

<sup>11</sup>*Dipartimento di Chimica, Università di Genova, Genova, Italy*

<sup>12</sup>*Paul Scherrer Institut (PSI), Villigen, Switzerland*

(Dated: March 28, 2025)

The determination of the absolute neutrino mass scale remains a fundamental open question in particle physics, with profound implications for both the Standard Model and cosmology. Direct kinematic measurements, independent of model-dependent assumptions, provide the most robust approach to address this challenge. In this Letter, we present the most stringent upper bound on the effective electron neutrino mass ever obtained with a calorimetric measurement of the electron capture decay of  $^{163}\text{Ho}$ . The HOLMES experiment employs an array of ion-implanted transition-edge sensor (TES) microcalorimeters, achieving an average energy resolution of 6 eV FWHM with a scalable, multiplexed readout technique. With a total of  $7 \times 10^7$  decay events recorded over two months and a Bayesian statistical analysis, we derive an upper limit of  $m_\beta < 27 \text{ eV}/c^2$  at 90% credibility. These results validate the feasibility of  $^{163}\text{Ho}$  calorimetry for next-generation neutrino mass experiments and demonstrate the potential of a scalable TES-based microcalorimetric technique to push the sensitivity of direct neutrino mass measurements beyond the current state of the art.

Measuring the mass of neutrinos or antineutrinos is one of the last critical tasks that need attention to complete the understanding of the Standard Model of elementary particles and their interactions. While next-generation neutrino experiments are expected to tackle the mass-ordering problem [1, 2], and the neutrinoless double beta decay searches probe the Majorana nature of neutrinos [3–6], only direct neutrino mass experiments can provide the definitive answer on the absolute mass scale. Additionally, increasing tensions with the oscillation experiment results make less reliable [7, 8] the neutrino mass derived from cosmological observations analysed within the framework of the  $\Lambda$ CDM model and its extensions. The strength of direct neutrino mass experiments is that they rely solely on the conservation of energy and momentum in weak nuclear beta decays to determine the neutrino mass observables which, for present-day experimental reach, are approximated by the effective (anti)neutrino mass  $m_\beta = \sqrt{\sum_{i=1,2,3} |U_{ei}^2| m_i^2}$ , where  $U_{ei}$  are the elements of the first row of the PMNS matrix and  $m_i$  are the masses of each neutrino mass eigenstate. Generally,

the signature of the neutrino mass is identified by a corresponding reduction in the total kinetic energy available to detectable particles. To date, experiments studying tritium beta decay have provided the most stringent limits on the antineutrino mass. The latest of these experiments, KATRIN, leverages magnetic adiabatic collimation with an electrostatic filter (MAC-E filter) to analyze the electrons emitted by a gaseous tritium source. KATRIN is currently taking data and is approaching its planned sensitivity of about 300 meV on the antineutrino mass [9]. At the same time, KATRIN is reaching the limit of its technique, and further improvements in the sensitivity of direct measurements require radically new developments. One such development is the KATRIN++ project, which aims to enhance KATRIN’s sensitivity by adopting low-temperature detectors for electron energy differential spectroscopy [10]. Proposed new techniques involve the use of Cyclotron Resonance Electron Spectroscopy (CRES) alone (Project8 [11] and QTNU [12]) or in combination with more advanced electron filtering techniques (PTOLEMY [13]), however, they are all at an embryonic stage. The most advanced of these, Project8,

has recently achieved a sensitivity of about 150 eV on the antineutrino mass [14].

An alternative experimental approach is provided by low-temperature microcalorimetry [15]. In this method, the decaying radionuclides are embedded within the absorber of low-temperature detectors, which are typically hundreds of microns in size. This configuration allows for high-resolution spectroscopy of the total energy released during the decay process, except for the portion carried away by neutrinos. Compared to integral spectrometry with MAC-E filters, this approach eliminates uncertainties related to the decay final states. Additionally, it detects decays with nearly 100% efficiency and, by measuring the spectrum in parallel in each detector, optimizes the usage of measuring time. These advantages together enable a faster accumulation of statistics. Furthermore, due to the fundamentally different systematic uncertainties [16, 17], calorimetry and the use of radioactive isotopes other than tritium make these experiments an ideal complement for strengthening the robustness of direct neutrino mass measurements.

First attempts involved the use of  $^{187}\text{Re}$  as the beta decaying isotope and achieved sensitivities around 20 eV on the antineutrino mass [18–20], but the lack of scalability ultimately led to the abandonment of more ambitious experimental plans. Subsequently, several new projects (HOLMES [21], ECHo [22], and NUMECS [23]) started to study the electron capture of  $^{163}\text{Ho}$  as proposed in [24].

In this letter, we present the first physics result of the HOLMES experiment [21], which improves upon the result from ECHo in [25] and establishes the calorimetric technique as the most mature and promising currently available for advancing direct neutrino mass sensitivity beyond KATRIN. Future sensitive  $^{163}\text{Ho}$  based neutrino mass experiments have the additional compelling potential to give valuable insights into differences between the neutrino and antineutrino masses, which would indicate CPT violation and have profound implications for the understanding of fundamental physics, as it would challenge the Standard Model and suggest new physics beyond it [26].

A calorimetric neutrino mass experiment using  $^{163}\text{Ho}$  measures the energy released – primarily through electrons [27] – following the electron capture (EC) decay:

$$^{163}\text{Ho} + e^- \rightarrow ^{163}\text{Dy} + \nu_e, \quad (1)$$

which features the lowest known  $Q$ -value (about 2863 eV [28]) and a half-life of approximately 4750 years, much shorter than that of  $^{187}\text{Re}$ , thereby yielding a higher specific activity that is more suitable for use in microcalorimeters. The  $^{163}\text{Ho}$  calorimetric spectrum, shown in Fig. 1, has as its outstanding feature a combination of Breit-Wigner shaped peaks at the binding energies of the atomic electrons which energy conservation allows to be captured (i.e. electrons in 3s shell, M1,

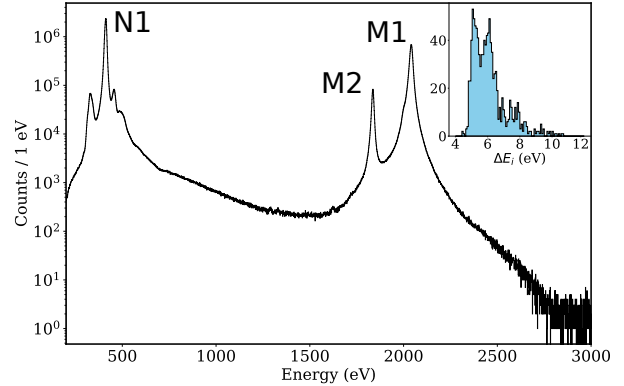


FIG. 1. The total recorded  $^{163}\text{Ho}$  calorimetric spectrum obtained summing about 1000 partial calibrated spectra measured with the HOLMES microcalorimeters. The spectrum contains about  $6 \times 10^7$  events above the 300 eV threshold. The top-right inset shows the distribution of the energy resolution (FWHM) of the individual partial spectra, evaluated from the noise equivalent power (NEP).

or above). Additional, fainter contributions are given by shake-up and shake-off atomic rearrangements following higher order excitations [29–32]. Although the full spectral shape is non-trivial and a full analytical description is still lacking, the region of interest (ROI) for the neutrino mass estimation – the endpoint of the spectrum – is remarkably smooth and shaped mostly by the phase space singularity. The lack of features at the endpoint is, indeed, a strong advantage of the calorimetric approach. The endpoint of the  $^{163}\text{Ho}$  spectrum is dominated by the right wing of the M1 peak at about 2041 eV and the exponential tail of the highest-energy shake-off.

HOLMES uses arrays of Transition Edge Sensor (TES) microcalorimeters [33] operated at a temperature of about 95 mK in a  $^3\text{He}/^4\text{He}$  dilution refrigerator. The  $^{163}\text{Ho}$  nuclei are ion-implanted at a shallow depth of approximately 100 Å in a  $(180 \times 180) \mu\text{m}^2$  gold layer (see Appendix A for details on isotope preparation and implantation) which is then covered with the deposition of a second overlapping gold layer. Both layers constitute the absorber of the microcalorimeter and each has a thickness of approximately 1  $\mu\text{m}$ , ensuring the full absorption of the radiation emitted in the decay, as required for a calorimetric measurement. The absorber is strongly thermally coupled to the TES sensor, allowing the detection of temperature variations induced by  $^{163}\text{Ho}$  decays. After completing the processing to embed the  $^{163}\text{Ho}$  source and to release the SiN membranes, which provide the tuned thermal coupling of the microcalorimeters to the heat bath [34], the ion implanted array is heat sunk in the gold plated copper box shown in Fig. 2, which is attached to the mixing chamber of the dilution refrigerator after all the electrical and thermal connections are made

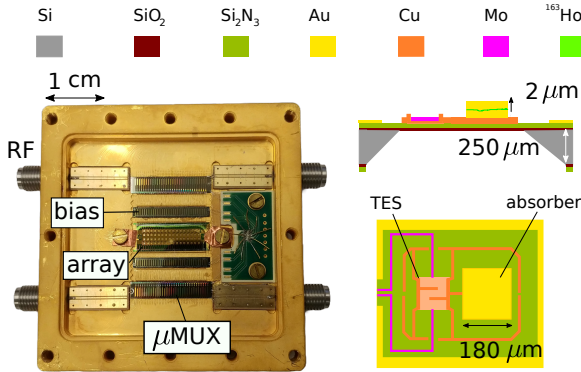


FIG. 2. Left: Copper box containing the 64 TES array in the middle. The two chips on either sides of the array are the bias network and the microwave multiplexer, respectively. The array dimensions are approximately  $(20 \times 10) \text{ mm}^2$ . The multiplexer has the feedline aligned with the SMA connectors used for feeding the readout tones. For readout, two SMAs on one side are connected via a short semirigid coaxial cable. Right: Schematic, not to scale, representation of the HOLMES TES microcalorimeter used in the experiment.

by ultrasonic bonding.

The experiment presented here employs an array of 64 TES microcalorimeters. These microcalorimeters are arranged in a  $16 \times 4$  matrix, as shown in Fig. 2, and their signals are frequency-multiplexed in the (4-8) GHz band, leveraging non-hysteretic rf-SQUIDs as current-to-frequency transducers, linearized through flux ramp modulation [35]. The multiplexed signals are recovered at room temperature using a heterodyne readout scheme (further technical details on the readout electronics can be found in Appendix B) and software-triggered pulses are stored on disk for further offline processing [36].

This microcalorimeter array, together with the multiplexed readout configuration, forms the foundational building block of our research program. The goal is to further develop and scale the current prototype in the coming years, ultimately leading to an experiment with enhanced statistical sensitivity in the sub-eV range.

When no  $^{163}\text{Ho}$  is implanted, the multiplexed HOLMES microcalorimeters designed, fabricated and measured as described above show an energy resolution of about 4 to 5 eV FWHM on the 6 keV X-ray line of manganese. Signals have an approximately double exponential shape with rise and decay times of about  $20 \mu\text{s}$  and  $600 \mu\text{s}$ , respectively.

In this Letter we report the results of the analysis of the data collected in two physics runs, lasting 2 months for a total live time exposure of about  $7 \times 10^4 \text{ detector} \times \text{hour}$  with about  $7 \times 10^7$   $^{163}\text{Ho}$  decays. Following the implantation, 48 detectors were found to exhibit non-zero activity, reaching up to 0.6 Bq, with an average activity of 0.27 Bq. The total activity of the array is approximately

15 Bq, corresponding to a source of about  $3.2 \times 10^{12}$   $^{163}\text{Ho}$  nuclei, i.e. about 0.9 ng.

The final spectrum analyzed (Fig. 1) for the neutrino mass is obtained by adding the spectra of the 48 active detectors, which, in turn, are obtained by joining their energy-calibrated partial spectra from data collected during periods lasting from 2 to 5 days. Additional information about the procedure adopted to calibrate the partial spectra are given in Appendix C.

The energies of the most prominent peaks in the  $^{163}\text{Ho}$  calorimetric spectrum – labeled as M1 (2040.8(3) eV), M2 (1836.4(8) eV) and N1(411.7(1) eV) in Fig. 1 – were measured during a dedicated run, in which the detectors were exposed to an X-ray source emitting the K lines of aluminum [37] and chlorine [38, 39]. The positions of the peaks are in very good agreement with those found in [40]. Since the amplitude of the signals of a TES is a slightly non-linear estimator of the energy of the event, the energy calibration of the raw  $^{163}\text{Ho}$  spectra is achieved by extrapolating the positions of the M1, M2 and N1 peaks with a quadratic binomial.

The energy resolutions measured in the calibrated spectra correlate as expected with the additional heat capacity introduced by  $^{163}\text{Ho}$  in the absorbers. They are primarily determined by the intrinsic detector noise and progressively degrade with increasing activities. The FWHM resolutions of all partial spectra have an average value of  $\langle \Delta E_{\text{FWHM}} \rangle = (6 \pm 1) \text{ eV}$ , with a minimum of approximately 4.4 eV.

The final spectrum, shown in Fig. 1 contains about  $6 \times 10^7$  events above the common analysis threshold set to about 300 eV and can be described by the expression

$$S_{\text{exp}} = \sum_i [N_i (\mathcal{S}_{\text{Ho}} + f_i^{pp} \mathcal{S}_{\text{Ho}}^{pp}) + \mathcal{B}_i] * \mathcal{R}_i \quad (2)$$

where  $\mathcal{S}_{\text{Ho}}$  is the true calorimetric EC energy spectral distribution in the calorimetric energy  $E_c$  and the summation is carried over all the calibrated partial spectra.  $\mathcal{S}_{\text{Ho}}^{pp}(E_c)$  is the true pile-up spectrum accounting for time unresolved  $^{163}\text{Ho}$  decays: it is given by the self-convolution of the calorimetric EC decay spectrum  $\mathcal{S}_{\text{Ho}}$  and extends up to twice the endpoint energy [16]. In first approximation, these events have a probability of  $f_i^{pp} = \tau_i^{\text{R}} A_i$ , where, for each of the  $i$ -th calibrated spectra,  $\tau_i^{\text{R}}$  and  $A_i$  are the detector time resolution [41] and implanted  $^{163}\text{Ho}$  activity, respectively. For the detectors of this work  $f_i^{pp} \lesssim 10^{-5}$ , thus making the contribution of the pile-up component in Eq. (2) negligible.  $N_i$  are normalization factors taking care of the  $^{163}\text{Ho}$  decays in each spectrum and  $\mathcal{B}_i(E_c)$  are the energy distributions of spurious events caused by the environmental radioactivity and cosmic rays which are estimated to be flat in the ROI [42]. Finally, in Eq. (2) the sum of the true spectra is convolved with detector energy response function  $\mathcal{R}_i(E_c)$  of  $i$ -th calibrated spectrum, which from detector characterization turns out to be simply Gaussian with FWHM

$$\Delta E_i.$$

Applying the properties of the convolution and for a constant background term, Eq. (2) can be rewritten as

$$\mathcal{S}_{\text{exp}} = [N_{\text{tot}}(\mathcal{S}_{\text{Ho}} + f_{\text{eff}}^{pp}\mathcal{S}_{\text{Ho}}^{pp})] * \mathcal{R}_{\text{eff}} + b_{\text{eff}} \quad (3)$$

with  $N_{\text{tot}} = \sum_i N_i$  and where the smallness and smoothness of the pile-up component and the present statistical uncertainty allow to introduce an average Gaussian response  $\mathcal{R}_{\text{eff}}(E_c) \simeq \mathcal{G}(E_c|0, \Delta E_{\text{eff}})$ , which approximates the true response functions coming from Eq. (2) with a deviation in shape estimated to be less than 2% in the  $[-\Delta E_{\text{eff}}, \Delta E_{\text{eff}}]$  interval. An additional implicit approximation already applied in Eq. (2) is the assumption of a perfectly linearized energy response of the detectors. However, the adopted quadratic binomial calibration remains an approximation which, when extrapolated to the ROI beyond the three interpolated calibration points (M1, M2, and N1), may introduce a non-trivial systematic distortion in the summed spectrum of Eq. (3). Applying the same three point calibration procedure to the measurements with the external calibration source, the residual nonlinearity in the detector energy responses is measured to cause deviations < 1% on the chlorine K $\alpha$  positions at about 2600 eV. Monte Carlo simulations demonstrate that the impact of all the above approximations on neutrino mass estimation is negligible compared to the current statistical fluctuations.

To perform a sensitive neutrino mass estimation with  $^{163}\text{Ho}$ , the ROI must be chosen *cum grano salis*. The upper energy limit should extend beyond the expected EC end point ( $E_0$ ) to constrain the background count rate per detector which is found to be  $(1.7 \pm 0.1) \times 10^{-4}/\text{eV/day}$  between 2900 eV and 3500 eV, consistent with the expectations [42]. The choice of the low energy limit, on the other hand, is a trade off. It must be low enough to allow for a precise statistical estimation of both  $m_\beta$  and  $E_0$ , yet close enough to the endpoint to ensure that the assumption of spectral smoothness holds, thereby enabling the description of  $^{163}\text{Ho}$  with only a few simple terms.

With the acquired statistics reported in this work, the ROI is chosen between 2250 eV and 3500 eV, where we find that the  $^{163}\text{Ho}$  true spectrum  $\mathcal{S}_{\text{Ho}}$  in Eq. (3) can be modelled as a sum of three terms (see also dashed lines in Fig. 3):

$$\mathcal{S}_{\text{Ho}} \approx \mathcal{S}'_{\text{Ho}} = k_0(k_{\text{BW}}\mathcal{S}_{\text{BW}} + k_{\text{SO}}\mathcal{S}_{\text{SO}} + \mathcal{S}_{\text{pol}}) \times \mathcal{F}_{\text{PS}}, \quad (4)$$

where  $k_0$ ,  $k_{\text{BW}}$  and  $k_{\text{SO}}$  take care of the overall unit normalization.  $\mathcal{S}_{\text{BW}}$  describes the right tail of the M1 line

$$\mathcal{S}_{\text{BW}}(E_c|\gamma, E_{\text{M1}}) = \frac{1}{2\pi} \frac{\gamma}{(E_c - E_{\text{M1}})^2 + \gamma^2/4}, \quad (5)$$

where  $E_{\text{M1}}$  and  $\gamma$  are the line position and FWHM, respectively.  $\mathcal{S}_{\text{SO}}$  describes the energy spectrum of a shake-

TABLE I. Pearson correlation coefficients between key parameters in the Bayesian fit.

	$E_0$	$m_\beta$	$\theta_0$	$N$	$k_{\text{BW}}$	$k_{\text{SO}}$	$\gamma$
$m_\beta$	0.40	-	-0.06	0.00	-0.01	-0.07	0.00
$E_0$	-	0.40	-0.16	0.04	0.00	-0.20	0.00

	$E_{\text{so}}$	$\tau_2$	$\tau_1$	$b_{\text{eff}}$	$\Delta E_{\text{eff}}$	$N_{\text{pp}}$
$m_\beta$	0.07	0.00	-0.13	0.00	0.00	0.00
$E_0$	0.27	-0.01	-0.50	-0.23	0.00	0.00

off de-excitation [30, 32], parametrized as

$$\begin{aligned} \mathcal{S}_{\text{SO}}(E_c|E_{\text{so}}, \tau_1, \tau_2) &= \\ &= \frac{1}{\tau_2 - \tau_1} \left( e^{-(E_c - E_{\text{so}})/\tau_2} - e^{-(E_c - E_{\text{so}})/\tau_1} \right), \end{aligned} \quad (6)$$

where  $E_{\text{so}}$ ,  $\tau_1$  and  $\tau_2$  are the shake-off transition energy, and the double exponential constants respectively.  $\mathcal{S}_{\text{pol}}(E_c)$  is a low degree polynomial, accounting for the tails of other peaks and shake-offs of the  $^{163}\text{Ho}$  spectrum which are out of the ROI. Indeed, we find that just a constant term  $\theta_0$  is enough,  $\mathcal{S}_{\text{pol}}(E_c|\vec{\theta}) \simeq \theta_0$ . Finally,  $\mathcal{F}_{\text{PS}}$  is the decay phase space factor, which is the only term that explicitly contains  $m_\beta$

$$\mathcal{F}_{\text{PS}}(E_c|m_\beta, E_0) = (E_0 - E_c)\sqrt{(E_0 - E_c)^2 - m_\beta^2} \quad (7)$$

To extract the  $m_\beta$  for the electron neutrino, we perform a Bayesian parameter estimation in the ROI using a Poisson likelihood (see Appendix D for details on parameter priors and fitting procedure) with the spectrum described by Eq. (3) and Eq. (4). The posterior is explored through a Hamiltonian Markov chain Monte Carlo using STAN [43]. There are 13 free parameters in the fit. Among these, only 10 can be constrained by the data in the chosen ROI, namely  $N$ ,  $k_{\text{BW}}$ ,  $k_{\text{SO}}$ ,  $E_0$ ,  $m_\beta$ ,  $E_{\text{so}}$ ,  $\tau_1$ ,  $\tau_2$ ,  $b_{\text{eff}}$ ,  $\theta_0$  (as shown in Fig. 6 in Appendix D).

It is worth emphasizing that, after parameter estimation, the posterior of the parameter of interest,  $m_\beta$ , is not directly correlated with any of the parameters describing the  $^{163}\text{Ho}$  spectrum, as shown in Table I, with the exception of  $E_0$  (see also Fig. 4). This is expected: the phase space factor  $\mathcal{F}_{\text{PS}}$  is the only term which contains  $m_\beta$  and the  $^{163}\text{Ho}$  spectrum is smooth at the end-point.

Finally, Fig. 4 shows the results of this fit procedure on the recorded data, which results in an upper limit for the electron neutrino mass of  $m_\beta < 27 \text{ eV}/c^2$  at 90% credibility. The endpoint is measured to be  $E_0 = 2848^{+7}_{-6} \text{ eV}$ , compatible with the value reported in [28].

The findings outlined here validate the approach first proposed more than 40 years ago in [24] and subsequently developed and implemented in recent years by

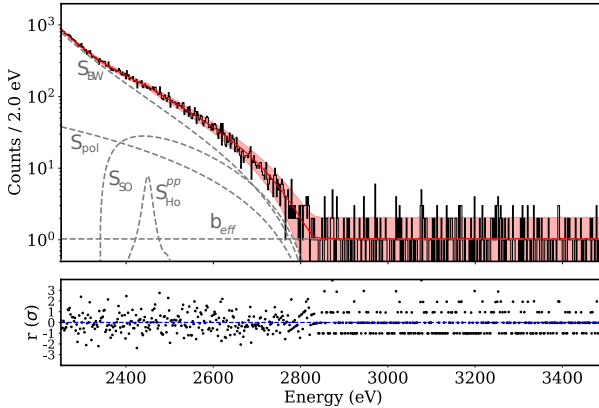


FIG. 3. Top: Results of the Bayesian analysis of the calorimetric  $^{163}\text{Ho}$  spectrum in the ROI with dashed lines showing the various components in Eq. (4). The red line and the reddish band represent the mean and standard deviation of the distribution of the generated data, following the posteriors. The bottom part shows the residuals  $r$  between the experimental data and the mean of the generated data, normalized by the standard deviation of the latter.

erated by leveraging modern microfabrication techniques to produce large-scale arrays with many thousands of detectors and by utilizing microwave multiplexing for the efficient readout of their signals, thereby exploiting the scalability needed for next-generation experiments. The high-statistics spectrum recorded here also enables a realistic sensitivity study that will define the final configuration for a next-generation neutrino mass experiment, aiming for sub-0.1 eV-scale sensitivity and opening the exploration of a range of neutrino masses that is presently inaccessible.

The HOLMES experiment has been supported by Istituto Nazionale di Fisica Nucleare (INFN) and by European Research Council under the European Union's Seventh Framework Programme (FP7/2007–2013)/ERC Grant Agreement no. 340321.

#### Appendix A: $^{163}\text{Ho}$ sample preparation and embedding

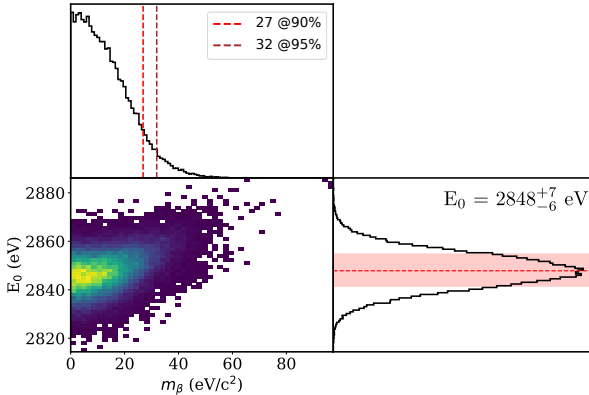


FIG. 4. Detail of the posteriors for  $m_\beta$  and  $E_0$  with their correlation as a result of the Bayesian analysis of the  $^{163}\text{Ho}$  calorimetric spectrum.

the HOLMES and ECHo collaborations. The new bound on the electron neutrino mass presented in this Letter is the strongest ever achieved studying the EC decay of  $^{163}\text{Ho}$ , positioning the experiment as one of the most promising candidates for next-generation neutrino mass measurements. Although extending the neutrino mass sensitivity of this approach to the 0.1 eV level requires increasing the overall statistics by a factor of about 10<sup>9</sup>, the scalability of the critical experimental parameters of the prototype presented here – namely, the number of detectors,  $^{163}\text{Ho}$  activity, and measuring time – renders this goal realistic for an experiment that maintains an almost table-top size. Given that all key components have now been validated, further progress can be accel-

The  $^{163}\text{Ho}$  isotope used in this work was produced by irradiating an  $^{162}\text{Er}$  enriched  $\text{Er}_2\text{O}_3$  sample with thermal neutrons in the high-flux nuclear reactor at the Institut Laue-Langevin (ILL, Grenoble, France). The produced  $^{163}\text{Ho}$  was extracted from the irradiated sample using radiochemical methods [44]. However, the chemically purified sample still contains a fraction of the beta-decaying isomer  $^{166m}\text{Ho}$  (about  $2 \times 10^{-3}$  Bq( $^{166m}\text{Ho}$ )/Bq( $^{163}\text{Ho}$ )) produced in the reactor and which must be removed to avoid excess background counts in the ROI. Isotope selection and ion implantation were performed by means of a dedicated system composed of a hot-running cold plasma sputter ion source coupled to a stirring magnet, a dipole magnet, and an adjustable slit.  $^{163}\text{Ho}$  ions exiting the ion source are accelerated to 30 kV, selected by the dipole and further filtered by the slit, finally impinging on the microcalorimeter array with a current of about 5 nA and a beam size of few millimeters FWHM [45]. The estimated separation of the  $^{163}\text{Ho}$  and  $^{166m}\text{Ho}$  beams when they hit the array is about  $6\sigma$ . During ion implantation, the thick photoresist mask used to pattern the  $180 \times 180 \mu\text{m}^2$  bottom gold layer was left in place to protect the rest of the array and was removed only after the deposition of the second gold layer. In order to obtain an approximately uniform  $^{163}\text{Ho}$  activity across the array, four implantation runs of about 3 h each were performed with the array shifted between runs by several millimeters with respect to the beam center. The  $^{163}\text{Ho}$  ion current was monitored throughout implantation by measuring the current flowing to ground through the gold layer covering the array.

## Appendix B: Detector array multiplexed readout

The signals of the 64 microcalorimeters are split and routed to two 32-channel rf-SQUID multiplexing chips, positioned along the two long sides of the microcalorimeter array (Fig. 2). These chips combine the frequency-converted signals into two 512 MHz-wide bands, starting at 4 GHz and 5 GHz, respectively. The multiplexed signals are transmitted through a single coaxial cable and amplified by a low-noise HEMT amplifier at 4 K. Signals from each multiplexing chip are recovered at room temperature using a Software-Defined Radio, implemented via two Reconfigurable Open Architecture Computing Hardware (ROACH2) boards [46], in a heterodyne scheme. These boards, equipped with ADC/DAC modules, are combined with two Intermediate Frequency boards for up- and down-conversion. Software-triggered pulses are stored in a RAID system for further offline processing [36].

## Appendix C: Data analysis

Each of the about 1000 recorded raw spectra has been calibrated with a sequence of steps which includes [36] 1) the rejection of spurious signals and too unstable time intervals, 2) the amplitude estimation by applying the optimal filter, 3) the gain time drift correction by monitoring the position of the M1, M2 and N1 peaks in the spectra, and 4) the energy calibration using the known positions of the same peaks. The well designed cryogenic environment combined with the off-line analysis ensures a duty cycle of 82% with a percentage of discarded events below 1% and, as shown in Fig. 5, a corrected gain stability well within the detector energy resolution over a few days. The events discarded using mild linear cuts on pulse shape parameters [36], optimized for the ROI, are primarily signals distorted by pile-up and background radiation interacting with components of the microcalorimeters other than the detector absorber.

## Appendix D: Bayesian parameter estimation

Bayesian fitting of the ROI using the model described by equations (2) to (7) involves estimating 13 parameters. For the analysis, we normalize the spectra in the ROI so that, instead of  $N_{tot}$  and  $f_{pp}^{eff}$ , we introduce  $N$  and  $N_{pp}$  which represent the number of decays and of pile-up events in the ROI, respectively. Data in the chosen ROI can constrain only 10 of the 13 parameters, namely  $N$ ,  $k_{BW}$ ,  $k_{SO}$ ,  $E_0$ ,  $m_\beta$ ,  $E_{so}$ ,  $\tau_1$ ,  $\tau_2$ ,  $b_{eff}$ ,  $\theta_0$ , as shown in Fig. 6. For these parameters, we use uninformative prior distributions with large standard deviations, while for the remaining 3 parameters,  $N_{pp}$ ,  $\Delta E_{eff}$ , and  $\gamma$ , we use weakly informative priors. The priors for the effective

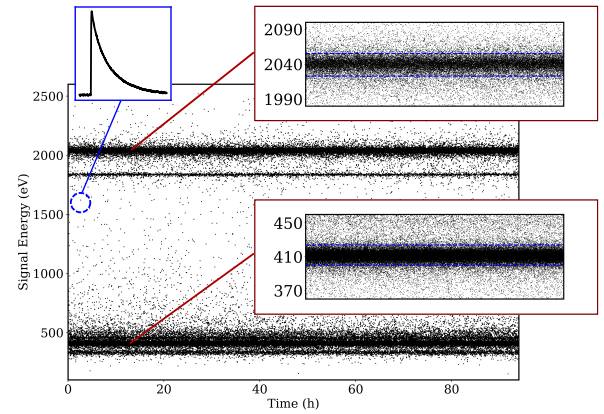


FIG. 5. Stability of the corrected energy gain over multiple days as shown by the events in the M and N peaks. The corrected gain drift remains well within the detector's energy resolution minimizing systematic uncertainties in the energy scale. The dashed lines in the insets on the right delimit a  $\pm\sigma$  region around the mean of the highlighted peak. The inset on the left shows an impulse from a  $^{163}\text{Ho}$  decay event.

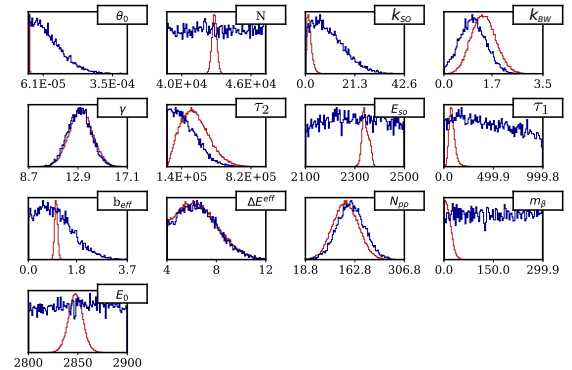


FIG. 6. Prior (blue) and posterior (red) distributions for the key fit parameters used in the Bayesian analysis. The fit parameters include the endpoint energy  $E_0$ , the neutrino mass  $m_\beta$ , and the other spectral shape parameters described in the text.

energy resolution  $\Delta E_{eff}$  in Eq. (2) and for  $N_{pp}$  are set to allow variations within reasonable ranges around the values expected from the measured  $\langle \Delta E_{FWHM} \rangle$  and the estimated  $f_{pp}$ , respectively. The peak marked  $S_{\text{Ho}}^{pp}$  in Fig. 3 comes from the self-convolution of the N and M peaks in the pile-up spectrum and its amplitude is too low to be constrained by the data. While the position of the M1 Breit-Wigner peak  $E_{M1}$  in Eq. (5) is fixed for simplicity to the value, its FWHM ( $\gamma$ ) is set to allow variation within a reasonable range. For both, we use the values obtained from our data as described above. Although the  $Q$ -value of  $^{163}\text{Ho}$  has been measured with high precision [28], it is considered good practice to treat

the endpoint  $E_0$  of the spectrum as a free parameter. Errors in the energy determination of the main peaks used for calibrating the summed spectrum could shift the fitted endpoint energy. This shift is accurately accounted for only if the endpoint is allowed to vary.

To verify the fidelity of the effective model of Eq. (4) in describing the  $^{163}\text{Ho}$  spectrum within the chosen ROI, we use Monte Carlo simulations. A set of  $n$  toy experiments is simulated. For each experiment the recorded data are resampled with statistical fluctuations, and each time a fit with the effective model (Eqs. 2 and 4) is performed to evaluate the upper limit for the 90% credible interval of  $m_\beta$ . The resulting distribution has a mean of  $40\text{ eV}/c^2$  and a standard deviation of  $10\text{ eV}/c^2$ , which is compatible with the result obtained from the real data.

R. H. Maruyama, D. Mayer, Y. Mei, N. Moggi, S. Manganini, T. Napolitano, M. Nastasi, J. Nikkel, C. Nones, E. B. Norman, A. Nucciotti, I. Nutini, T. O'Donnell, J. L. Ouellet, S. Pagan, C. E. Pagliarone, L. Pagnanini, M. Pallavicini, L. Pattavina, M. Pavan, G. Pessina, V. Pettinacci, C. Pira, S. Pirro, S. Pozzi, E. Previtali, A. Puiu, C. Rosenfeld, C. Rusconi, M. Sakai, S. Sangiorgio, B. Schmidt, N. D. Scielzo, V. Sharma, V. Singh, M. Sisti, D. Speller, P. T. Surukuchi, L. Taffarello, F. Terranova, C. Tomei, K. J. Vetter, M. Vignati, S. L. Wagaarachchi, B. S. Wang, B. Welliver, J. Wilson, K. Wilson, L. A. Winslow, S. Zimmermann, S. Zucchelli, and CUORE Collaboration, *NATURE* **604**, 53 (2022).

- [5] M. Agostini, G. R. Araujo, A. M. Bakalyarov, M. Balata, I. Barabanov, L. Baudis, C. Bauer, E. Bellotti, S. Belogurov, A. Bettini, L. Bezrukov, V. Biancacci, D. Borowicz, E. Bossio, V. Bothe, V. Brudanin, R. Brugnera, A. Caldwell, C. Cattadori, A. Chernogorov, T. Comelato, V. D'Andrea, E. V. Demidova, N. Di Marco, E. Doroshkevich, F. Fischer, M. Fomina, A. Gangapshev, A. Garfagnini, C. Gooch, P. Grabmayr, V. Gurentsov, K. Gusev, J. Hakenmüller, S. Hemmer, R. Hiller, W. Hofmann, J. Huang, M. Hult, L. V. Inzhechik, J. Janicskó Csáthy, J. Jochum, M. Junker, V. Kazalov, Y. Kermaïdic, H. Khushbakht, T. Kihm, I. V. Kirpichnikov, A. Klimenko, R. Kneißl, K. T. Knöpfle, O. Kochetov, V. N. Kornoukhov, P. Krause, V. V. Kuzminov, M. Laubenstein, A. Lazzaro, M. Lindner, I. Lippi, A. Lubashevskiy, B. Lubsandorzhiev, G. Lutter, C. Macolino, B. Majorovits, W. Maneschg, L. Manzanillas, M. Miloradovic, R. Mingazheva, M. Misiaszek, P. Moseev, Y. Müller, I. Nemchenok, K. Panas, L. Pandola, K. Pelczar, L. Pertoldi, P. Piseri, A. Pullia, C. Ransom, L. Rauscher, S. Riboldi, N. Rumyantseva, C. Sada, F. Salamida, S. Schönert, J. Schreiner, M. Schütt, A.-K. Schütz, O. Schulz, M. Schwarz, B. Schwingenheuer, O. Selivanenko, E. Shevchik, M. Shirchenko, L. Shtembari, H. Simgen, A. Smolnikov, D. Stukov, A. A. Vasenko, A. Veresnikova, C. Vignoli, K. Von Sturm, T. Wester, C. Wiesinger, M. Wojcik, E. Yanovich, B. Zatschler, I. Zhitnikov, S. V. Zhukov, D. Zinatulina, A. Zschocke, A. J. Zsigmond, K. Zuber, G. Zuzel, and GERDA Collaboration, *Physical Review Letters* **125**, 252502 (2020).
- [6] G. Anton, I. Badhrees, P. S. Barbeau, D. Beck, V. Belov, T. Bhatta, M. Breidenbach, T. Brunner, G. F. Cao, W. R. Cen, C. Chambers, B. Cleveland, M. Coon, A. Craycraft, T. Daniels, M. Danilov, L. Darroch, S. J. Daugherty, J. Davis, S. Delaquis, A. Der Mesrobian-Kabakian, R. DeVoe, J. Dilling, A. Dolgonenko, M. J. Dolinski, J. Echevers, W. Fairbank, D. Fairbank, J. Farine, S. Feyzbakhsh, P. Fierlinger, D. Fudenberg, P. Gautam, R. Gornea, G. Gratta, C. Hall, E. V. Hansen, J. Hoessl, P. Hufschmidt, M. Hughes, A. Iverson, A. Jamil, C. Jessiman, M. J. Jewell, A. Johnson, A. Karulin, L. J. Kaufman, T. Koffas, R. Krücken, A. Kuchenkov, K. S. Kumar, Y. Lan, A. Larson, B. G. Lenardo, D. S. Leonard, G. S. Li, S. Li, Z. Li, C. Licciardi, Y. H. Lin, R. MacLellan, T. McElroy, T. Michel, B. Mong, D. C. Moore, K. Murray, O. Njoya, O. Nusair, A. Odian, I. Ostrovskiy, A. Piepke, A. Pocar, F. Retière, A. L. Robinson, P. C. Rowson, D. Ruddell, J. Runge, S. Schmidt, D. Sinclair, A. K. Soma, V. Stekhanov, M. Tarka, J. Todd, T. Tolba, T. I. Totev, B. Veenstra, V. Veeraraghavan, P. Vogel, J.-L. Vuilleumier, M. Wagenpfeil, J. Watkins,

\* matteo.borghesi@unimib.it

† angelo.nucciotti@unimib.it

‡ dan.schmidt@nist.gov

§ joel.ullom@nist.gov

[1] The Juno Collaboration, *Chinese Physics C* **49**, 033104 (2025).

[2] The DUNE collaboration, *The European Physical Journal C* **80**, 978 (2020).

[3] KamLAND-Zen Collaboration, S. Abe, S. Asami, M. Eizuka, S. Futagi, A. Gando, Y. Gando, T. Gima, A. Goto, T. Hachiya, K. Hata, S. Hayashida, K. Hosokawa, K. Ichimura, S. Ieki, H. Ikeda, K. Inoue, K. Ishidoshiro, Y. Kamei, N. Kawada, Y. Kishimoto, M. Koga, M. Kurasawa, N. Maemura, T. Mitsui, H. Miyake, T. Nakahata, K. Nakamura, K. Nakamura, R. Nakamura, H. Ozaki, T. Sakai, H. Sambonsugi, I. Shimizu, J. Shirai, K. Shiraishi, A. Suzuki, Y. Suzuki, A. Takeuchi, K. Tamae, K. Ueshima, H. Watanabe, Y. Yoshida, S. Obara, A. K. Ichikawa, D. Chernyak, A. Kozlov, K. Z. Nakamura, S. Yoshida, Y. Takemoto, S. Umehara, K. Fushimi, K. Kotera, Y. Urano, B. E. Berger, B. K. Fujikawa, J. G. Learned, J. Maricic, S. N. Axani, J. Smolsky, Z. Fu, L. A. Winslow, Y. Efremenko, H. J. Karwowski, D. M. Markoff, W. Tornow, S. Dell'Oro, T. O'Donnell, J. A. Detwiler, S. Enomoto, M. P. Decker, C. Grant, A. Li, and H. Song, *Physical Review Letters* **130**, 051801 (2023).

[4] D. Q. Adams, C. Alduino, K. Alfonso, F. T. Avignone, III, O. Azzolini, G. Bari, F. Bellini, G. Benatto, M. Beretta, M. Biassoni, A. Branca, C. Brofferio, C. Bucci, J. Camilleri, A. Caminata, A. Campani, L. Canonica, X. G. Cao, S. Capelli, L. Cappelli, L. Cardani, P. Carniti, N. Casali, E. Celi, D. Chiesa, M. Clemenza, S. Copello, O. Cremonesi, R. J. Creswick, A. D'Addabbo, I. Dafinei, S. Dell'Oro, S. Di Domizio, V. Dompe, D. Q. Fang, G. Fantini, M. Faverzani, E. Ferri, F. Ferroni, E. Fiorini, M. A. Franceschi, S. J. Freedman, S. H. Fu, B. K. Fujikawa, A. Giachero, L. Gironi, A. Giuliani, P. Gorla, C. Gotti, T. D. Gutierrez, K. Han, E. Hansen, V. K. M. Heeger, R. G. Huang, H. Z. Huang, J. Johnston, G. Keppel, Y. G. Kolomensky, C. Ligi, R. Liu, L. Ma, Y. G. Ma, L. Marini,

- M. Weber, L. J. Wen, U. Wicherki, G. Wrede, S. X. Wu, Q. Xia, D. R. Yahne, L. Yang, Y.-R. Yen, O. Ya. Zeldovich, T. Ziegler, and EXO-200 Collaboration, *Physical Review Letters* **123**, 161802 (2019).
- [7] S. Gariazzo, O. Mena, and T. Schwetz, *Physics of the Dark Universe* **40**, 101226 (2023).
- [8] D. Wang, O. Mena, E. Di Valentino, and S. Gariazzo, *Updating neutrino mass constraints with Background measurements* (2024), arXiv:2405.03368 [astro-ph, physics:hep-ph].
- [9] M. Aker, A. Beglarian, J. Behrens, A. Berlev, U. Besserer, B. Bieringer, F. Block, S. Bobien, M. Böttcher, B. Bornschein, L. Bornschein, T. Brunst, T. S. Caldwell, R. M. D. Carney, L. La Cascio, S. Chilingaryan, W. Choi, K. Debowski, M. Deffert, M. Descher, D. Díaz Barrero, P. J. Doe, O. Dragoun, G. Drexlin, K. Eitel, E. Ellinger, R. Engel, S. Enomoto, A. Felden, J. A. Formaggio, F. M. Fränkle, G. B. Franklin, F. Friedel, A. Fulst, K. Gauda, W. Gil, F. Glück, R. Grössle, R. Gumbsheimer, V. Gupta, T. Höhn, V. Hannen, N. Haußmann, K. Helbing, S. Hickford, R. Hiller, D. Hillesheimer, D. Hinz, T. Houdy, A. Huber, A. Jansen, C. Karl, F. Kellerer, J. Kellerer, M. Kleifges, M. Klein, C. Köhler, L. Köllenberger, A. Kopmann, M. Korzeczek, A. Kovalík, B. Krasch, H. Krause, N. Kunka, T. Lasserre, T. L. Le, O. Lebeda, B. Lehnert, A. Lokhov, M. Machatschek, E. Malcherek, M. Mark, A. Marsteller, E. L. Martin, C. Melzer, A. Menshikov, S. Mertens, J. Mostafa, K. Müller, H. Neumann, S. Niemes, P. Oelpmann, D. S. Parno, A. W. P. Poon, J. M. L. Poyato, F. Priester, S. Ramachandran, R. G. H. Robertson, W. Rodejohann, M. Röllig, C. Rötteler, C. Rodenbeck, M. Ryšavý, R. Sack, A. Saenz, P. Schäfer, A. Schaller née Pollithy, L. Schimpf, K. Schlösser, M. Schlösser, L. Schlüter, S. Schneidewind, M. Schrank, B. Schulz, A. Schwemmer, M. Šefčík, V. Sibille, D. Siegmann, M. Slezák, F. Spanier, M. Steidl, M. Sturm, M. Sun, D. Tcherniakhovski, H. H. Telle, L. A. Thorne, T. Thümmler, N. Titov, I. Tkachev, K. Urban, K. Valerius, D. Vénos, A. P. Vizcaya Hernández, C. Weinheimer, S. Welte, J. Wendel, J. F. Wilkerson, J. Wolf, S. Wüstling, J. Wydra, W. Xu, Y.-R. Yen, S. Zadorogny, G. Zeller, and The KATRIN Collaboration, *Nature Physics* **18**, 160 (2022).
- [10] N. Kovac, F. Adam, S. Kempf, M.-C. Langer, M. Müller, R. Sack, M. Schlösser, M. Steidl, and K. Valerius, *Comparison of the detector response and calibration function of metallic microcalorimeters for X-ray photons and external electrons* (2025), arXiv:2502.05975 [physics].
- [11] A. A. Esfahani, D. M. Asner, S. Böser, R. Cervantes, C. Claessens, L. De Viveiros, P. J. Doe, S. Doeelman, J. L. Fernandes, M. Fertl, E. C. Finn, J. A. Formaggio, D. Furse, M. Guigue, K. M. Heeger, A. M. Jones, K. Kazkaz, J. A. Kofron, C. Lamb, B. H. LaRoque, E. Machado, E. L. McBride, M. L. Miller, B. Montreal, P. Mohanmurthy, J. A. Nikkel, N. S. Oblath, W. C. Pettus, R. G. H. Robertson, L. J. Rosenberg, G. Rybka, D. Rysewyk, L. Saldaña, P. L. Slocum, M. G. Sternberg, J. R. Tedeschi, T. Thümmler, B. A. VanDevender, L. E. Vertatschitsch, M. Wachtendonk, J. Weintrob, N. L. Woods, A. Young, and E. M. Zayas, *Journal of Physics G: Nuclear and Particle Physics* **44**, 054004 (2017).
- [12] A. A. S. Amad, F. F. Deppisch, M. Fleck, J. Gallop, T. Goffrey, L. Hao, N. Higginbotham, S. D. Hogan, S. B. Jones, L. Li, N. McConkey, V. Monachello, R. Nichol, J. A. Potter, Y. Ramachers, R. Saakyan, E. Sedzielewski, D. Swinnock, D. Waters, S. Withington, S. Zhao, and J. Zou, *Determining Absolute Neutrino Mass using Quantum Technologies* (2024), arXiv:2412.06338 [hep-ex].
- [13] M. Betti, M. Biasotti, A. Boscá, F. Calle, N. Canci, G. Cavoto, C. Chang, A. Cocco, A. Colijn, J. Conrad, N. D'Ambrosio, N. De Groot, P. De Salas, M. Faverzani, A. Ferella, E. Ferri, P. Garcia-Abia, I. García-Cortés, G. Gomez-Tejedor, S. Gariazzo, F. Gatti, C. Gentile, A. Giachero, J. Gudmundsson, Y. Hochberg, Y. Kahn, A. Kievsky, M. Lisanti, C. Mancini-Terracciano, G. Mangano, L. Marcucci, C. Mariani, J. Martínez, M. Messina, A. Molinero-Vela, E. Monticone, A. Moroño, A. Nucciotti, F. Pandolfi, S. Parlati, S. Pastor, J. Pedrós, C. De Los Heros, O. Pisanti, A. Polosa, A. Puiu, I. Rago, Y. Raitses, M. Rajteri, N. Rossi, I. Rucandio, R. Santorelli, K. Schaeffner, C. Tully, M. Viviani, F. Zhao, and K. Zurek, *Journal of Cosmology and Astroparticle Physics* **2019** (7).
- [14] Project 8 Collaboration, A. Ashtari Esfahani, S. Böser, N. Buzinsky, M. C. Carmona-Benitez, C. Claessens, L. de Viveiros, P. J. Doe, M. Fertl, J. A. Formaggio, J. K. Gaison, L. Gladstone, M. Grando, M. Guigue, J. Hartse, K. M. Heeger, X. Huyan, J. Johnston, A. M. Jones, K. Kazkaz, B. H. LaRoque, M. Li, A. Lindman, E. Machado, A. Marsteller, C. Matthé, R. Mohiuddin, B. Montreal, R. Mueller, J. A. Nikkel, E. Novitski, N. S. Oblath, J. I. Peña, W. Pettus, R. Reimann, R. G. H. Robertson, D. Rosa De Jesús, G. Rybka, L. Saldaña, M. Schram, P. L. Slocum, J. Stachurska, Y.-H. Sun, P. T. Surukuchi, J. R. Tedeschi, A. B. Telles, F. Thomas, M. Thomas, L. A. Thorne, T. Thümmler, L. Tvrznikova, W. Van De Pontseele, B. A. VanDevender, J. Weintrob, T. E. Weiss, T. Wendler, A. Young, E. Zayas, and A. Ziegler, *Physical Review Letters* **131**, 102502 (2023).
- [15] A. Nucciotti, *Advances in High Energy Physics* **2016**, 1 (2016).
- [16] A. Nucciotti, *The European Physical Journal C* **74**, 3161 (2014).
- [17] A. Nucciotti, E. Ferri, and O. Cremonesi, *Astroparticle Physics* **34**, 80 (2010).
- [18] C. Arnaboldi, C. Brofferio, O. Cremonesi, E. Fiorini, C. Lo Bianco, L. Martensson, A. Nucciotti, M. Pavan, G. Pessina, S. Pirro, E. Previtali, M. Sisti, A. Giuliani, B. Margesin, and M. Zen, *Physical Review Letters* **91**, 161802 (2003).
- [19] M. Sisti, C. Arnaboldi, C. Brofferio, G. Ceruti, O. Cremonesi, E. Fiorini, A. Giuliani, B. Margesin, L. Martensson, A. Nucciotti, M. Pavan, G. Pessina, S. Pirro, E. Previtali, L. Soma, and M. Zen, *Nuclear Instruments and Methods in Physics Research Section A: Accelerators, Spectrometers, Detectors and Associated Equipment* **520**, 125 (2004).
- [20] F. Gatti, *Nuclear Physics B - Proceedings Supplements Neutrino* **2000**, 91, 293 (2001).
- [21] B. Alpert, M. Balata, D. Bennett, M. Biasotti, C. Boragno, C. Brofferio, V. Ceriale, D. Corsini, P. K. Day, M. De Gerone, R. Dressler, M. Faverzani, E. Ferri, J. Fowler, F. Gatti, A. Giachero, J. Hays-Wehle, S. Heinitz, G. Hilton, U. Köster, M. Lusignoli, M. Maino, J. Mates, S. Nisi, R. Nizzolo, A. Nucciotti, G. Pessina, G. Pizzigoni, A. Puiu, S. Ragazzi, C. Reintsema, M. R.

- Gomes, D. Schmidt, D. Schumann, M. Sisti, D. Swetz, F. Terranova, and J. Ullom, [The European Physical Journal C](#) **75**, 112 (2015).
- [22] L. Gastaldo, K. Blaum, K. Chrysalidis, T. Day Goodacre, A. Domula, M. Door, H. Dorrer, Ch. E. Düllmann, K. Eberhardt, S. Eliseev, C. Enss, A. Faessler, P. Filianin, A. Fleischmann, D. Fonnesu, L. Gamer, R. Haas, C. Hassel, D. Hengstler, J. Jochum, K. Johnston, U. Kebschull, S. Kempf, T. Kieck, U. Köster, S. Lahiri, M. Maiti, F. Mantegazzini, B. Marsh, P. Neroutsos, Yu. N. Novikov, P. C. O. Ranitzsch, S. Rothe, A. Rischka, A. Saenz, O. Sander, F. Schneider, S. Scholl, R. X. Schüssler, Ch. Schweiger, F. Šimkovic, T. Stora, Z. Szűcs, A. Türler, M. Veinhard, M. Weber, M. Wegner, K. Wendt, and K. Zuber, [The European Physical Journal Special Topics](#) **226**, 1623 (2017).
- [23] M. P. Croce, M. W. Rabin, V. Mocko, G. J. Kunde, E. R. Birnbaum, E. M. Bond, J. W. Engle, A. S. Hoover, F. M. Nortier, A. D. Pollington, W. A. Taylor, N. R. Weisse-Bernstein, L. E. Wolfsberg, J. P. Hays-Wehle, D. R. Schmidt, D. S. Swetz, J. N. Ullom, T. E. Barnhart, and R. J. Nickles, [Journal of Low Temperature Physics](#) **184**, 958 (2016).
- [24] A. De Rújula and M. Lusignoli, [Physics Letters B](#) **118**, 429 (1982).
- [25] C. Velte, F. Ahrens, A. Barth, K. Blaum, M. Braß, M. Door, H. Dorrer, Ch. E. Düllmann, S. Eliseev, C. Enss, P. Filianin, A. Fleischmann, L. Gastaldo, A. Goeggemann, T. D. Goodacre, M. W. Haverkort, D. Hengstler, J. Jochum, K. Johnston, M. Keller, S. Kempf, T. Kieck, C. M. König, U. Köster, K. Kromer, F. Mantegazzini, B. Marsh, Yu. N. Novikov, F. Piquemal, C. Riccio, D. Richter, A. Rischka, S. Rothe, R. X. Schüssler, Ch. Schweiger, T. Stora, M. Wegner, K. Wendt, M. Zampaolo, and K. Zuber, [The European Physical Journal C](#) **79**, 1026 (2019).
- [26] C. A. Moura and F. Rossi-Torres, [Universe](#) **8**, 42 (2022).
- [27] The total fluorescence yield is expected to be of the order of  $10^{-4}$ .
- [28] C. Schweiger, M. Braß, V. Debierre, M. Door, H. Dorrer, C. E. Düllmann, C. Enss, P. Filianin, L. Gastaldo, Z. Harman, M. W. Haverkort, J. Herkenhoff, P. Indelicato, C. H. Keitel, K. Kromer, D. Lange, Y. N. Novikov, D. Renisch, A. Rischka, R. X. Schüssler, S. Eliseev, and K. Blaum, [Nature Physics](#) **20**, 921 (2024).
- [29] R. G. H. Robertson, [Physical Review C](#) **91**, 035504 (2015), arXiv:1411.2906 [hep-ph, physics:nucl-th, physics:physics].
- [30] A. De Rújula and M. Lusignoli, [Journal of High Energy Physics](#) **2016**, 15 (2016).
- [31] A. Faessler, L. Gastaldo, and F. Šimkovic, [Physical Review C](#) **95**, 045502 (2017).
- [32] M. Brass and M. W. Haverkort, [New Journal of Physics](#) **22**, 093018 (2020).
- [33] B. Alpert, D. Becker, D. Bennet, M. Biasotti, M. Borghesi, G. Gallucci, M. De Gerone, M. Faverzani, E. Ferri, J. Fowler, J. Gard, A. Giachero, J. Hays-Wehle, G. Hilton, J. Mates, A. Nucciotti, A. Orlando, G. Pessina, A. Puiu, C. Reintsema, D. Schmidt, D. Swetz, J. Ullom, and L. Vale, [The European Physical Journal C](#) **79**, 304 (2019).
- [34] M. Borghesi, B. Alpert, M. Balata, D. Becker, D. Bennet, E. Celasco, N. Cerboni, M. De Gerone, R. Dressler, M. Faverzani, M. Fedkevych, E. Ferri, J. Fowler, G. Gallucci, J. Gard, F. Gatti, A. Giachero, G. Hilton, U. Koster, D. Labranca, M. Lusignoli, J. Mates, E. Maugeri, S. Nisi, A. Nucciotti, L. Origo, G. Pessina, S. Ragazzi, C. Reintsema, D. Schmidt, D. Schumann, D. Swetz, J. Ullom, and L. Vale, [Nuclear Instruments and Methods in Physics Research Section A: Accelerators, Spectrometers, Detectors and Associated Equipment](#) **1051**, 168205 (2023).
- [35] D. Becker, D. Bennett, M. Biasotti, M. Borghesi, V. Ceriale, M. D. Gerone, M. Faverzani, E. Ferri, J. Fowler, G. Gallucci, J. Gard, A. Giachero, J. Hays-Wehle, G. Hilton, J. Mates, A. Nucciotti, A. Orlando, G. Pessina, A. Puiu, C. Reintsema, D. Schmidt, D. Swetz, J. Ullom, and L. Vale, [Journal of Instrumentation](#) **14** (10), P10035.
- [36] M. Borghesi, *Toward the First Neutrino Mass Measurement of Holmes*, Ph.D. thesis, University of Milano-Bicocca, Milano, Italy (2022).
- [37] J. Schweppe, R. Deslattes, T. Mooney, and C. Powell, [Journal of Electron Spectroscopy and Related Phenomena](#) **67**, 463 (1994).
- [38] J. A. Bearden, [Reviews of Modern Physics](#) **39**, 78 (1967).
- [39] M. O. Krause and J. H. Oliver, [Journal of Physical and Chemical Reference Data](#) **8**, 329 (1979).
- [40] P. C.-O. Ranitzsch, C. Hassel, M. Wegner, D. Hengstler, S. Kempf, A. Fleischmann, C. Enss, L. Gastaldo, A. Herlert, and K. Johnston, [Physical Review Letters](#) **119**, 122501 (2017).
- [41] We find that the time resolution of our detectors is completely independent of the implanted activity. It is primarily determined by the signal sampling time, approximately a few  $\mu\text{s}$ , which is therefore better than the signal rise time.
- [42] M. Borghesi, [The European Physical Journal Plus](#) **139**, 10.1140/epjp/s13360-024-04981-y (2024).
- [43] Stan Development Team, Stan Reference Manual, version 2.34.1, <https://mc-stan.org> (<https://mc-stan.org/docs/2.34/cmdstan-guide/index.html>) (2024).
- [44] S. Heinitz, N. Kivel, D. Schumann, U. Köster, M. Balata, M. Biasotti, V. Ceriale, M. De Gerone, M. Faverzani, E. Ferri, G. Gallucci, F. Gatti, A. Giachero, S. Nisi, A. Nucciotti, A. Orlando, G. Pessina, A. Puiu, and S. Ragazzi, [PLOS ONE](#) **13**, e0200910 (2018).
- [45] M. De Gerone, A. Bevilacqua, M. Borghesi, N. Cerboni, G. Ceruti, G. De Bodin De Galembert, M. Faverzani, M. Fedkevych, E. Ferri, G. Gallucci, F. Gatti, A. Giachero, E. Maugeri, P. Manfrinetti, A. Nucciotti, L. Parodi, G. Pessina, S. Ragazzi, D. Schumann, and F. Siccardi, [Nuclear Instruments and Methods in Physics Research Section A: Accelerators, Spectrometers, Detectors and Associated Equipment](#) **1051**, 168168 (2023).
- [46] S. McHugh, B. A. Mazin, B. Serfass, S. Meeker, K. O'Brien, R. Duan, R. Raffanti, and D. Werthimer, [Review of Scientific Instruments](#) **83**, 044702 (2012).